# Geothermal Play-Fairway Analysis of Washington State Prospects

**Corina Forson[1], Michael W. Swyer[2], Gina M. Schmalzle[3], Jessica L. Czajkowski[1], Trenton T. Cladouhos[2], Nicholas Davatzes[4], David K. Norman[1], and Ryan A. Cole[5]**

**[1]Washington Division of Geology and Earth Resources, Olympia, WA**
**[2]AltaRock Energy, Inc., Seattle, WA**
**[3]BOS Technologies, LLC, Seattle, WA**
**[4]Temple University, EES, Beury Hall, Philadelphia, PA**
**[5]Minerals and Geology Management, U.S. Forest Service, Missoula MT**

***Keywords***

*Play-Fairway, Washington, Mount St. Helens seismic zone, Wind River valley, Mount Baker, geothermal favorability, heat, permeability, GIS modeling*

## ABSTRACT

Analysis of existing geologic, geophysical, and geochemical data revealed areas with elevated heat and permeability, defining three promising plays along the central axis of the magmatic arc of Washington State: Mount St. Helens, Wind River valley, and the southeast flank of Mount Baker. These areas are geothermal 'fairways', or locations with high geothermal resource potential based on modeling. This project applies innovative data analyses (*Poly3D*) in conjunction with methods proven in previous geothermal favorability studies (ArcGIS and MATLAB) to extract new value from existing public data. Heat and permeability potential models for each play are weighted using the Analytical Hierarchy Process, and combined to map geothermal resource potential and locations for further data collection at each site. Heat potential is based on: (1) temperature gradients, (2) volcanic vents, (3) Quaternary intrusive rocks, (4) spring temperature, and (5) spring geothermometry. Permeability potential is based on: (1) slip and (2) dilation tendency on mapped and seismic faults (3) maximum shear strain rate, and (4) dilatational strain rate at the surface, (5) modeled fault displacement distribution, and (6) displacement gradient, (7) shear, and (8) tensile fracture density, and (9) local geology and geophysical data. This information is vital for revealing the small scale heat and permeability potential of each study area, locating areas of undiscovered or untapped resources, and reducing the risk and cost involved in greenfield exploration and development. Preliminary analysis of the three play areas shows promise for geothermal development. Uncertainty modeling is underway and the results will guide future exploration plans.

## Introduction

A pivotal step in development of a potential geothermal resource is the ability to successfully identify sites for exploration wells. The high cost and high risk associated with drilling a new well require that all factors influencing well productivity/injectivity are considered and that uncertainty is minimized. A comprehensive analysis of the geologic, geochemical, structural, and geophysical properties of the study area are crucial when addressing this challenge. The goal of this study is to provide valuable, quantitative analysis regarding the geothermal potential and to delineate profitable areas for further exploration in three plays along the Cascade magmatic arc: Mount St. Helens, Wind River valley and the southeast flank of Mount Baker (Fig. 1).

The Cascade Range in Washington State is home to some of the most active volcanic centers in the United States. Geothermal activity associated with the magmatic arc is typically expressed as hot springs and fumaroles. The region is tectonically dynamic and structurally complex; as demonstrated by frequent seismicity, historic volcanic eruptions, ongoing subduction, and active faults. However, the massive amount of precipitation, dense vegetation, and high relief in the western part of the state can mask surface manifestations as well as dampen the thermal signature of magmatic heat sources, conventionally detected through remote sensing, and thus act as one barrier to geothermal development. Despite the high geothermal favorability in Washington (Fig. 1; Boschmann and others, 2014), there are no current geothermal energy development projects in the state, making it impossible to test modeling parameters against known resources in the northern Cascades volcanic arc.

The modeling results presented in this paper are for the Mount St. Helens study area— the Wind River valley and Mount Baker heat and permeability models are currently underway and are not presented in this paper.

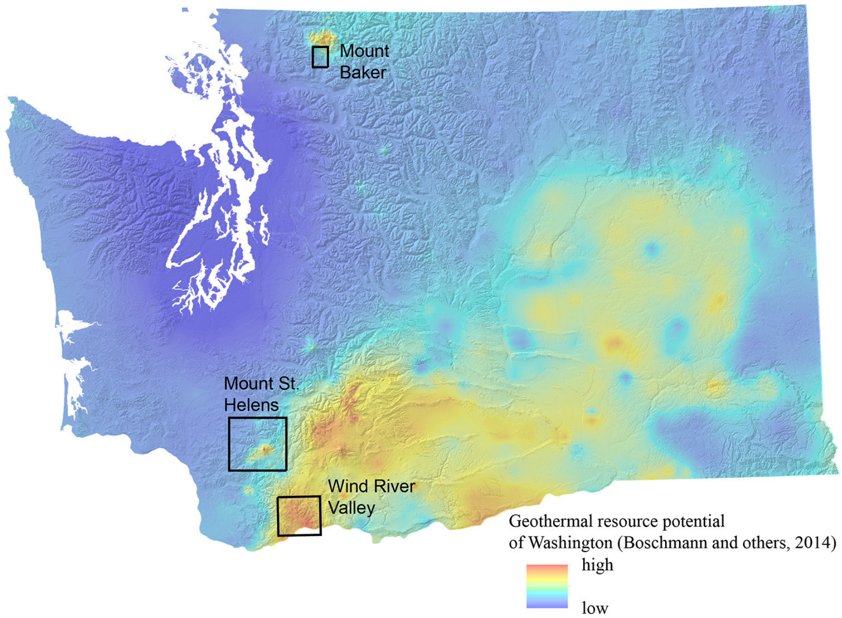


**Figure 1.** Geothermal resource potential map of Washington State by Boschmann and others (2014) based on variables of heat and permeability. Locations of the three play fairways in this study are outlined in black: Mount St. Helens, Wind River valley, and Mount Baker.

## Background

The Cascade magmatic arc is the result of oblique (northeast directed) subduction of the Juan de Fuca plate beneath the North American plate. GPS derived secular velocity estimates of the Pacific Northwest show the Oregon Coast Range Block is rotating clockwise with respect to stable North America, causing crustal extension in the backarc and contraction in central Washington (Wells and others, 1998; McCaffrey and others, 2000b; McCaffery and others, 2007). Voluminous, albeit discontinuous, volcanism accompanies subduction, and is expressed as a chain of active volcanoes along the crest of the Cascades. In addition to volcanism, the Washington State Cascade Range is also host to active faulting and abundant seismicity in the upper crust, likely related to complex subduction, block rotation, and active volcanism. The three study areas (Fig. 1) are all located within the Cascade magmatic arc, however, each occupy different geologic and tectonic settings, as briefly discussed below.

## Geologic Settings

*Mount St. Helens* (MSH) is located along the western front of the Cascade Range in southwest Washington (Fig. 1 and Fig. 2A). The frequency and scale of the eruptions at MSH over the last few thousand years make it currently the most active volcano in the Cascades (Sherrod and others, 2008). MSH lies along a 100-km-long zone of moderate (up to 5.5) magnitude earthquakes that have predominantly strike-slip focal mechanisms along north-striking fault planes. This band of seismicity is referred to as the St. Helens seismic zone (SHZ) (Weaver and Smith, 1983; Weaver and others, 1987). Interestingly, no surface trace has been identified along the trend of the SHZ (Evarts and others, 1987). The focal mechanism-determined motion along the SHZ is right-lateral strike-slip. A right step in the SHZ beneath the volcanic center generates a zone of extension between the offset faults. MSH is centered on this dextral offset, and the earthquake swarms occurring there are likely related to volcanic eruptions (Weaver and others, 1987). Weaver and others (1987) mapped SHZ faults from the seismicity surrounding MSH—the permeability modeling employed in this study expands on this premise and also uses seismicity to map fault planes at depth in this area.

The MSH volcano is the site of ongoing geothermal activity, expressed in part by numerous hot springs and fumaroles located in the central crater, along the northern flank, and on the debris flow and the pyroclastic deposits north of the 1980 flank collapse (henceforth referred to as "the Pumice Plain"). The fumaroles and springs located within the crater are likely connected directly to a magmatic heat source, while Pumice Plain springs are "rootless", meaning they are not connected directly to the magmatic source of heat or gas. Spring chemistry trends and alteration mineralogy from this area support this idea (Keith and others, 1981, Shevenell and Goff, 1995). For this reason, the Pumice Plain springs were excluded from this analysis. Four temperature gradient wells were drilled in the MSH study area, the highest recorded gradient is 50°C/km (Fig. 2A).

The *Wind River Valley***,** located in southwestern Washington, is a northwest-trending valley draining southeastward into the Columbia River near Washington's southern border (Fig. 1 and Fig. 2B). There are numerous thermal and mineral springs and seeps along and adjacent to this valley, several of which are developed into resorts. Several temperature-gradient wells drilled in the early 1980s yielded gradients as high as 160°C/km (Fig. 2B; Czajkowski and others, 2014c), and some water wells at the southern end of the valley, near the town of Carson, contain warm water. Detailed investigations with emphasis on the geothermal resources of the Wind River valley include Berri and Korosec (1983) and Czajkowski and others (2014a). There are numerous minor vents in the area, the youngest is Trout Creek Hill with a reported K-Ar age of 0.34 $\pm$ 0.07 Ma (Korosec, 1984, Berri and Korosec, 1983). Czajkowski and others (2014a) identified two dominant sets of faults in the area; northwest striking faults (such as the Wind River fault), and northeast striking faults (such as the Shipherds fault zone) (Fig. 2B). Based upon the presence of thermal and mineral springs, high temperature gradients, and warmer water along the valley's axis, it is proposed that an intersection of the northeast and northwest faults channel geothermal fluids from depth to the near surface within and along the length of this valley.

The *Mount Baker* study area is located on the southeast flank of Mount Baker, in northern Washington (Fig. 1 and Fig. 2C). Mount Baker is a Quaternary stratovolcano on the western front of the North Cascades. It is located within the Mount Baker–Snoqualmie National Forest, much of which is designated a national wilderness area. However, the location of the Mount Baker study area was in large part chosen based on current or nominated geothermal leases by the U.S. Forest Service (Fig. 2C).

The Mount Baker volcano and surrounding area have received attention from the geothermal community due to the presence of thermal features and young volcanic centers. Exploration activities have included detailed geologic mapping, spring sampling, geophysical surveys, soil mercury measurements, and limited temperature-gradient drilling (Korosec, 1984). Chemical geothermometry of Baker Hot Springs suggests that reservoir equilibrium temperature of this system may reach as high as 150° to 170°C (Korosec, 1984). In 1983, a 140-m deep (460 ft) temperature-gradient well was drilled near Baker Hot Springs. It had a bottomhole temperature of 48°C and a geothermal gradient between 200° and 309°C/km (Czajkowski and others, 2014c). However, this gradient is likely affected by hot spring circulation and may not represent a typical background value for the area.

## Fairway Mapping Methods

A geothermal reservoir requires that heat, permeability, and saturated porosity are present to provide adequate heat exchange, and are collocated at depths accessible by modern drilling technologies. Significant reservoir permeability enables thermal fluids to migrate freely through a reservoir and into a wellbore. This study will generate maps of the most favorable combinations of heat and permeability, and identify uncertainties within these categories for the three target areas. By combining measurements of the strain field from GPS velocities with a model of fault geometry and slip using *Poly3D* (Thomas, 1993), a boundary element modeling code, we hope to identify the most critically stressed structures in each area and understand how their displacement causes localized permeability enhancement. The underlying premise is that permeability is generally promoted by slip or opening of fractures, especially in conditions of low confining pressure and favorable geology. By modeling these conditions, we provide new detailed constraints of the relative permeability potential. *Poly3D* models faults/fractures/cavities as displacement discontinuities discretized into triangular elements in an elastic half-space to simulate fault slip and surrounding rock deformation. This technique has a strong dependence on detailed fault geometry and the regional strain field, and helps in identifying the most favorable locations for drilling discovery wells. The permeability models focus on two depths within the crust, 200 m (typical temperature gradient well depth), and 3 km (typical production well depth for this region). The permeability changes drastically between these two depths because many of the surface faults are not the same as faults delineated by seismicity at depth, which often have no surface expression.

The heat model is relatively straightforward; it models heat potential at the surface based on volcanic vents, hot springs, geothermometry, Quaternary intrusive rocks, and temperature gradient data. The heat model does not account for differences in heat at 200 m vs. 3 km, due to the lack of heat flow data. The innovative permeability modeling approach combined with conventional techniques for heat potential mapping were used to improve the resolution of the statewide geothermal assessment, and attempts to provide metrics for the dimensions of the potential reservoir. Two resource potential maps will be produced for each play, illustrating the potential for a geothermal reservoir at 200 m depth and 3 km depths. In addition, this approach can be refined for specific plays by validation against independent evidence from springs or geothermal alteration at the surface.

ArcGIS is used for data processing and modeling to incorporate the heat and fluid data for the three study areas, for weighting heat inputs by value (temperature, distance, lithology, type, etc.), for interpolation between points, and for combining and normalizing the various input data. Unless specified, the tools used in the ArcGIS modeling are from ESRI. MATLAB is used to model fault geometries from earthquake data and to calculate slip and dilation tendency which are highly dependent on fault geometry. *Poly3D* is used to model ongoing fault displacement and stress perturbation in larger volumes surrounding faults. This analysis requires knowledge of the orientation and magnitude of the current stress/strain rates at each play area. The GPS strain rates derived at the surface (data acquired from the Plate Boundary Observatory) are used as an initial constraint to derive the 3D, quasi-static, strain tensors at depth. In addition to constraining the boundary conditions for *Poly3D*, the strain rate was used to map maximum shear strain rate and dilational strain rate at the surface. All of the heat and permeability data are combined for favorability mapping in ArcGIS by normalizing each of the input layers, and assigning them weights according to expert opinion in the geothermal industry using the Analytical Hierarchy Process (AHP) (Saaty, 2008; Goepel, 2013).

## Heat Potential Model

The multi-criteria heat potential model is composed of the weighted sum of five intermediate rasters: (1) temperature gradient, (2) volcanic vent proximity, (3) intrusive rock proximity, (4) proximity to springs weighted by temperature, and (5) proximity to springs weighted by geothermometry inferred temperature. Temperature-gradient wells were compiled from the Washington Division of Geology and Earth Resources (WADGER) geothermal well database (Czajkowski, 2014), published data (Huang and Pollack, 1998; Fairbank and Faulkner, 1992; Jessop and others, 2005), and Southern Methodist University's Western Geothermal Areas Database (Blackwell, 2010). In large areas where no temperature gradients have been measured, a WADGER database of bottomhole-temperature data from water wells (Czajkowski, 2014c) was combined with average surface temperature (Gass, 1982) to calculate synthetic temperature gradients. The areal surficial extents of young silicic intrusive rock bodies were obtained from WADGER 1:100,000-scale digital geologic map data (WADGER, 2010a) and geologic mapping by Hildreth and others (2003). Spatial and attribute data for volcanic vents and springs were obtained from recent compilations from WADGER (Czajkowski and others, 2014b; Czajkowski and Bowman, 2014). Much of the data cited above was submitted to the National Geothermal Data System. Geothermometry temperatures for springs were calculated using the liquid geothermometer spreadsheets of Powell and Cumming (2010). All heat potential data and mapped faults for each of the three study areas are shown in Figure 2.

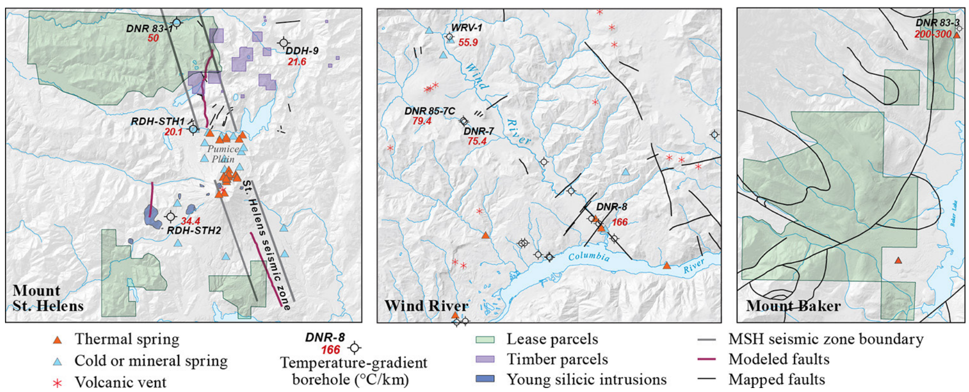


**Figure 2.** Shaded relief maps of each of the three play-fairway areas showing the model input layers and important features discussed in text.

### *Data Processing for Heat Potential Layers*

*Temperature gradient* values across the state were used in the initial temperature-gradient analysis. Kriging interpolation was used to predict continuous temperature-gradient values across the state (Fig. 3A). *Volcanic vents* point data were buffered into polygons, sized by vent type as follows: stratovolcanoes = 5 mi (8 km), calderas = 3 mi (4.8 km), and minor vents = 1.5 mi (2.4 km). Individual buffer polygons for stratovolcanoes, calderas, and minor vents were separately converted to weighted rasters with the raster value equal to the product of age weight and rock type weight. Separately,

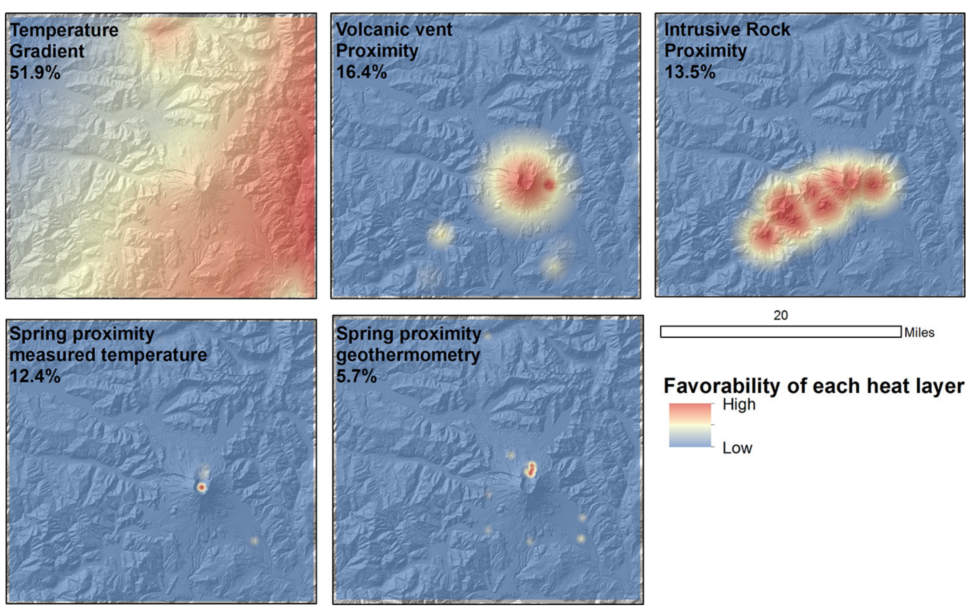


**Figure 3.** MSH area heat potential layers. Rasters are interpolated from point data. Weights assigned to each of the layers for use with the weighted sum tool in the combined heat raster are shown as percentages on each input layer.

Euclidean distance analyses were performed on individual minor vents, stratovolcanoes, and calderas. The minor vents, stratovolcano and caldera weighted rasters were multiplied by their respective reclassified distance rasters. Finally, the caldera, stratovolcano, and minor vent group rasters were combined using the fuzzy 'OR' overlay tool (Fig. 3B). *Intrusive rock proximity* used mapped late Pliocene to Holocene intrusive rhyodacitic to andesitic polygons, with an applied buffer of 3 mi (4.8 km). Euclidean distance analysis was performed on these polygons to generate the resultant proximity raster (Fig. 3C). S*pring proximity:* For both spring temperature (Fig. 3D) and spring geothermometry (Fig. 3E), springs were broken out individually, and then buffered to a distance of 0.5 mi (0.8 km). Non-overlapping buffered polygon were then individually converted to weighted rasters with the raster value equal to the spring temperature. Separately, Euclidean distance analyses were performed on non-overlapping springs, to generate the resultant distance rasters. The weighted temperature rasters were then multiplied by the distance rasters. All of the individual spring rasters were then mosaicked.

### *Combining Heat Potential Layers*

Weights assigned to each heat input raster were based on individual inputs from experienced geothermal professionals that were combined using the AHP (Saaty, 2008; Goepel, 2013) (example of the MSH study area rasters shown in Fig. 3). The five inputs were then combined using the weighted sum tool in ArcGIS.

## Permeability Potential Model

The multi-criteria permeability potential model is composed of the weighted sum of nine intermediate model rasters: (1) slip and (2) dilation tendency on mapped and seismically inferred faults (3) maximum shear strain rate, and (4) dilational strain rate at the surface, (5) fault displacement distribution, and (6) displacement gradient, (7) shear, and (8) tensile fracture density, and (9) local geology and geophysical data. Parameters 1-6 are modeled from faults mapped at the surface, seismicity, and GPS derived strain rate data; parameters 7&8 are derived from GPS velocity data; and parameter 9 is observed. Fault data were compiled from the DGER 1:100,000-scale digital surface geology, 1:500,000-scale digital surface geology, and active faults data within the digital seismogenic features database (WADGER, 2010a, b; Bowman and Czajkowski, 2014). Earthquake hypocenter locations were taken from the DGER seismogenic features database (Bowman and Czajkowski, 2014), originally obtained from the Pacific Northwest Seismic Network (PNSN), along with available earthquake focal mechanisms.

The permeability potential model examines both the fault plane (mapped on the surface and interpolated to depth, or inferred from seismicity) and the area around the fault. In the case of MSH, the magma chamber geometry beneath the volcano and a stress induced by deflation accompanying historic eruption is also included in the model based on the work of Barker and Malone (1991).

### *Model Configuration*

Modeling of the permeability potential requires (1) the geometry of the faults (and for MSH, the geometry of the magma chamber), (2) specified tractions, or burgers vector (displacement discontinuity) on their respective surfaces, and (3) remote stress/strain rate boundary conditions. In this study, the faults are modeled as surfaces of zero residual shear traction and zero normal displacement discontinuity. The magma chamber at MSH similarly sustains zero residual shear traction, but the normal traction corresponds to a pressure drop associated with eruption as per Barker and Malone (1991). In addition, the Earth's surface is treated as traction free, and in these initial models is flat. The 3D remote strain rate is modeled from GPS station velocities; here our focus is to use the strain rate to infer the anisotropy of the elastic strain tensor.

*3D Fault Geometry:* The fault geometry at depth was constrained with relocated seismicity from the Pacific Northwest Seismic Network. Planes were fit to events by fitting lines to multiple cross-sections along strike using Locally Weighted Scatterplot Smoothing (LOWESS, Burkey, 2008). For the MSH model, lines (faults) were fit to pre-1990 events at cross sections 300 m apart and at 300-m depth intervals, then re-iterated using both the pre-1990 fit points and post-1990 events. The points were then used to create a 3D mesh of triangular fault elements representing the fault surface (example: north fault in Fig. 4).

*Remote Strain Rate Tensor***:** The remote strain rate tensor was estimated using GPS derived secular velocities. GPS velocities were estimated using three component GPS time series from the National Science Foundation (NSF) Earthscope's Plate Boundary Observatory (PBO). The spline in tension method (Wessel and Bercovicci, 1998) was used to interpolate the GPS velocity field for each component using a tension of 0.3 and a grid size of 0.04° (the preferred tension and grid size of Hackl and others, 2009). The displacement gradients in the north and east direction for the north and east velocity components are estimated, and the symmetric infinitesimal strain rate tensor is derived, following the method of Hackl and others (2009). The components of the infinitesimal strain rate tensors up to 10 km outside the model area were averaged, and the two eigenvalues were used as the two principal horizontal strains. The vertical strain rate was determined using

Hooke's Law using a Poisson's ratio of 0.25 (Chou and Pagano, 1967). The three principal components of the 3D strain tensor used as the remote boundary are:

$$\epsilon_H = -0.0136\ (az.\ 72) \qquad \epsilon_h = 0.0181\ (az.\ 162) \qquad \epsilon_V = -0.0011$$

To account for stress changes with depth, the Young's modulus was changed for each modeled depth (4.2 GPa at 200m, and 71.7 GPa at 3km) so that when it is multiplied by $\epsilon_v$ it equals the vertical stress from the overlying rock.

*Fault Element Boundary Conditions:* For the fault elements, the shear traction was set to zero which simulates slip on a frictionless fault, and the normal displacement was set to zero, which prevents the fault from opening or the fault walls from interpenetrating. These boundary conditions provide an end-member case for the stress change induced by fault slip.

*Magma Chamber Boundary Conditions:* The magma chamber is a triangulated ellipsoid with dimensions and location following Barker and Malone (1991) which was fit to an aseismic gap under the MSH crater (Fig. 4). Like the faults, the elements of the magma chamber were given zero shear traction, but the normal direction was given a traction equal to the lithostatic stress of the magma chamber at each observation depth, which is less than the surrounding rock.

## *Model Results*

The faults, magma chamber, and corresponding local and remote boundary conditions are implemented in *Poly3D* to derive permeability potential both along the modeled faults and in the surrounding volume. On the fault itself these include the static slip and dilation tendency as well as the modeled displacement discontinuity and gradient of displacement. In the surrounding volume, these include the maximum horizontal Coulomb shear stress and least compressive principal stress. In addition, the dilation and maximum shear strain rate are modeled from GPS velocities and strain rates for all of Washington and Oregon and are modeled at a higher resolution across the entirety of each study area. These parameters are assessed on observation planes at 200 m and 3 km depth (Fig. 4) where they are the basis of weighted rasters used for the favorability maps. The relationship of these parameters to permeability potential is described below.

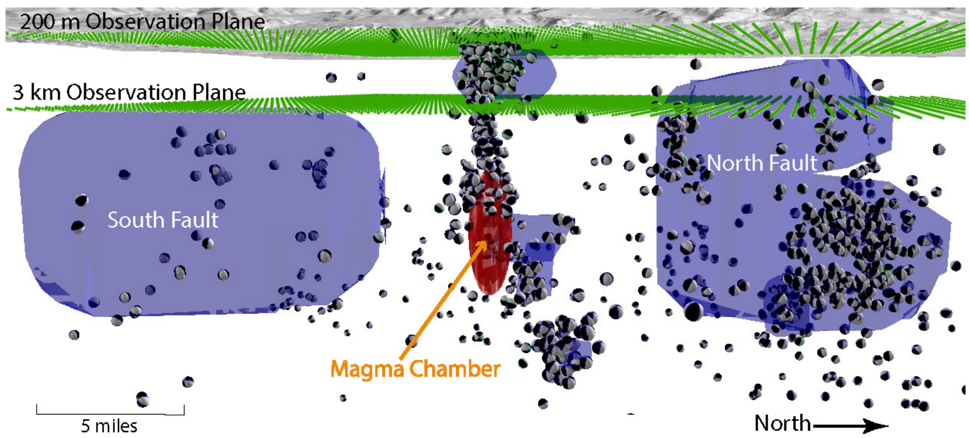


**Figure 4.** 3D fault model (looking west) with faults in blue, magma chamber in red, observation planes in green, and earthquake focal mechanisms shown in 3D. The north fault and the south fault cross only 3km observation plane, whereas the fault to the west behind the magma chamber near the surface crosses both the 200m and 3km observation planes.

## *Fault-Related Outputs*

*Displacement* is the magnitude of fault parallel (shear) displacement discontinuity across the fault surface in meters (Fig. 5A). Higher levels are typically associated with development of a low permeability fault core and a surrounding damage zone of potentially higher permeability (e.g., Caine and others, 1996) This allows the fault to act as a barrier to cross-fault flow, but to possibly conduct fluids parallel to the fault plane.

*Displacement gradient* is the change in slip along the fault surface divided by distance along fault surface between fault elements (Fig. 5B). High displacement gradients occur at the fault tips or where mechanical interaction with other, nearby slipping fault segments is strong (intersections/overlaps). Higher slip gradients reveal strain and a corresponding concentration of stress that is likely to correlate with damage in or adjacent to the fault. If this damage takes the form of dilating shear or tensile fractures this should promote permeability along the fault (Childs and others, 1995; Willemse and others, 1996).

*Slip tendency ($T_s$)* is the ratio of static shear to normal traction resolved on a fault surface by the remote stress/strain (Morris and others, 1996) (Fig. 5C). The shear and normal tractions are highly dependent on the local fault attitude relative to the remote stress tensor. A higher slip tendency means the fault has a higher potential for slip, although the effect of nearby faults is neglected. An advantage of this method is that it primarily depends on the fault geometry and anisotropy of the remote stress tensor, rather than the magnitude of the principal stresses which are more difficult to constrain in detail. If the slip tendency exceeds the coefficient of static friction on the fault surface, then the fault will slip. Faults with higher slip tendencies tend to act as fluid conduits, whereas faults with low slip tendencies can potentially block groundwater flow, or compartmentalize the reservoir.

*Dilation tendency ($T_d$)* is the ratio of the difference between the most compressive principal stress ($\sigma_1$) and the normal traction, and the difference between the most compressive principal stress and the least compressive principal stress ($\sigma_3$) (Ferrill and others, 1999) (Fig. 5D). Similar to slip tendency, this ratio is based on the static stress tensor. Where dilation tendency is at its maximum value of 1, then the fault surface is perpendicular to $\sigma_3$ and has the highest potential for opening. In a strike slip fault setting, this generally corresponds to a near vertical fault. Open faults and fractures can host large amounts of fluid flow, and fractures increase their flowrate as a cubic function of fault aperture according to the cubic law for fractures (Zoback, 2007).

### *Stress/Strain-Related Outputs*

*Maximum Coulomb shear stress ($S_c$)* is the potential for shear fracture failure in a volume of rock based on a Mohr-Coulomb failure criterion, which in a strike-slip setting is most apparent in the horizontal plane. The value is used as a proxy for fault/fracture density (Childs and others, 1995; Maerten and others, 2002). As $S_c$ increases, more orientations of potential shear fractures reach their strength threshold, which has the potential to both increase the density of fractures as well as promote connectivity. This in turn implies potential for a more convoluted flow path and therefore greater heat exchange between the reservoir rock and circulating fluids (Fig. 5E).

*Sigma 3 ($\sigma_3$)* is the least compressive principal stress (i.e., confining pressure) (Fig. 5F). A lower $\sigma_3$ both promotes dilation during slip of fractures and a higher potential for tensile failure. A negative $\sigma_3$ indicates tension and fracture opening.

*Dilatational strain rate ($\delta$)* is derived from GPS and reveals areas that are contracting or extending, and can be used to identify areas of active thrust or normal faulting (Hackl and others, 2009) (Fig. 5G).

*Maximum shear strain rate* derived from GPS indicates active strike-slip faults, as motion along faults is related to shear on that structure (Hackl and others, 2009) (Fig. 5H).

### *Raster Processing of Structural and Deformation Metrics Into Permeability Potential*

The outputs from MATLAB and *Poly3D* at both depth slices of 200 m and 3 km are point data with values representing the various parameters at a grid spacing of 2,000 ft (610 m). The points were then interpolated using an inverse distance weighting (IDW) process. The outputs from GPS strain rate data are generated using Generic Mapping Tools and have a NetCDF format that were reclassified using a bilinear resampling technique. Each of the aforementioned parameters defines a raster layer (Fig. 5) for use in predicting permeability potential.

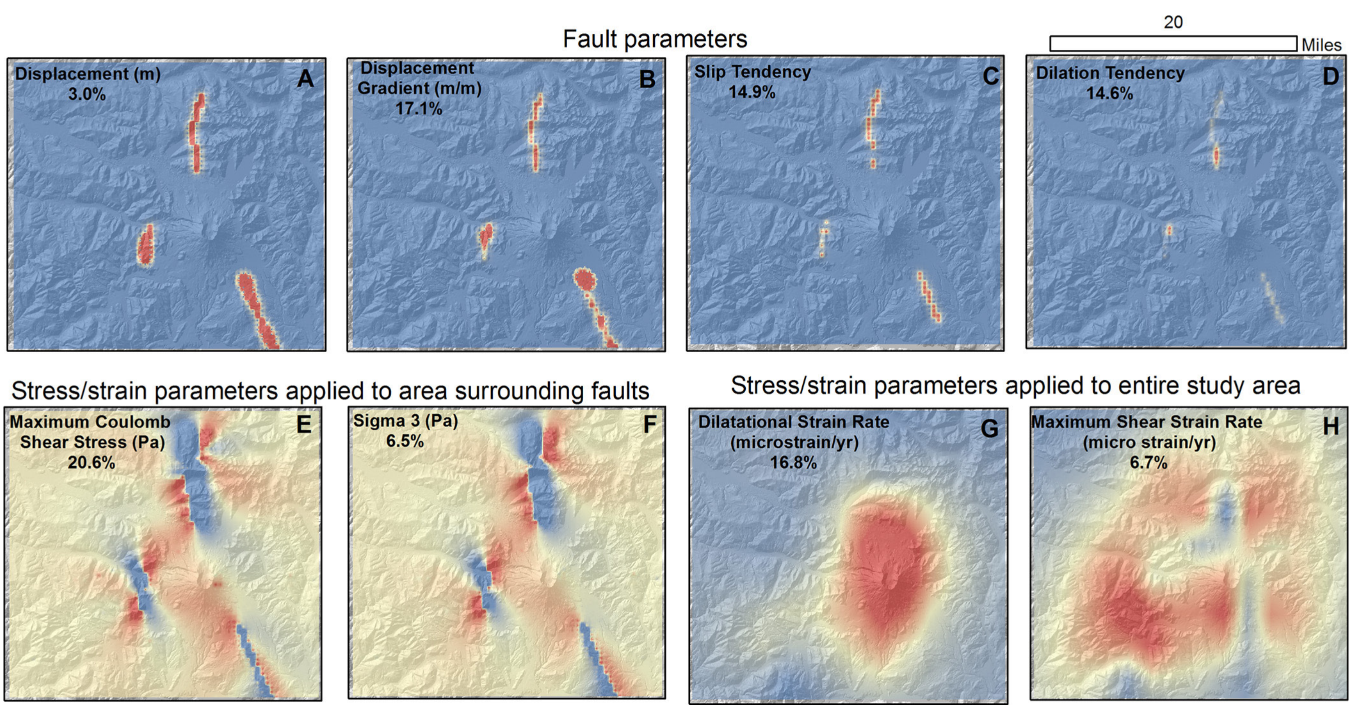


**Figure 5.** MSH study area permeability potential layers at 3 km depth. Rasters are interpolated from point data (raster processing discussed in data processing section). A-D are parameters modeled along the fault plane, E-F are parameters applied to the area surrounding the fault and G-H are regional parameters affecting permeability. Warmer colors indicate a higher potential for enhanced permeability. Weights assigned to each of the layers for use with the weighted sum tool in the combined permeability raster are shown on each map as percentages.

### *Combining Permeability Potential Layers*

The permeability inputs were then combined using the weighted sum tool in ArcGIS. The weights assigned to each heat input raster were based on the individual input from experienced geothermal professionals and the weights were combined using the AHP (Saaty, 2008; Goepel, 2013). The weights of each individual permeability input are shown in Figure 5 as percentages.

### *Geothermal Play-Fairway Resource Potential Model*

The geothermal play-fairway resource potential models represent the relative geothermal potential at each of the three plays based on the weighted sum of the permeability and heat potential models. These models characterize geothermal resource potential without consideration of regulatory restrictions, land-management restrictions, or economic viability. In addition to the assumptions inherent in the permeability potential and heat potential models, the resource potential model assumes that areas with coincident elevated permeability and heat will have higher favorability for future exploration. The final individual heat and permeability (at both 200 m and 3 km depths) potential models, as well as the combined heat and permeability layers for the MSH study area are shown below in Figure 6.

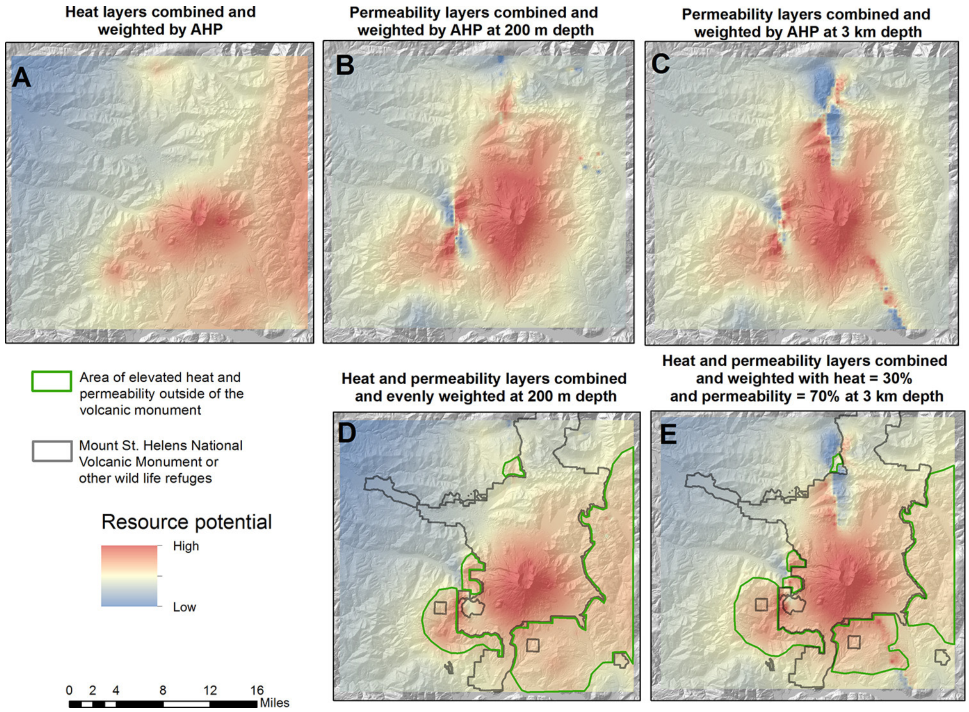


**Figure 6.** Resource favorability models for the MSH study area. A) Heat potential model based on the weights shown in Figure 3 B) Permeability potential model at 200 m depth based on the weights shown in Figure 5. C) Permeability potential model at 3 km depth based on the weights shown in Figure 5. D) Heat and permeability layers combined and weighed evenly at 200 m depth. E) Heat and permeability layers combined and weighed evenly at 3 km depth. In D and E green polygons show general areas of high potential for future exploration outside of the MSH National Volcanic Monument (black outline).

## Discussion

The resource potential models for the MSH study area distinguish zones with high geothermal potential at depths of 200 m and 3 km (outlined in green in Fig. 6 D and E). As expected, the MSH volcano shows high favorability, in large part due to the high weight assigned to volcanic vents and Quaternary intrusives in the heat potential model, along with the high weight assigned to dilatational strain rate, and maximum Coulomb shear stress in the permeability model (all are favorable directly centered on MSH, Fig. 3 and 5). Additionally, the SHZ is located along the axis of MSH and contributes to the permeability potential in that area. It should be mentioned that some areas, particularly the northwest part of the study area, data are sparse and therefore there is low favorability based on lack of data (as seen by the existing data points in Fig. 2).

Although there is not a drastic difference between the 200m and 3km combined heat and permeability maps (Fig. 6 D and E) there are subtle differences. The main contrast is seen in areas where the faults cross the 3km observation plane but not the 200m plane (Fig. 6 B and C). Because the heat potential is only modeled at the surface (due to the lack of temperature data that can be interpolated to depth) the heat input for the combined favorability does not change and this causes some of the similarities seen in each of the resource potential maps.

When compared to the original statewide assessment (Fig. 1) the focused study of the MSH area adds detail as well as highlight new areas of resource favorability based on the innovative permeability modeling and the refined heat potential modeling. The primary difference between the two assessments is that the statewide model did not look as in depth at the permeability potential. The statewide permeability potential was based on fault proximity, fault intersections, and earthquake density. This new detailed study of MSH models faults based on seismicity, in addition to using the mapped faults at the surface, and incorporates local and regional stress and strain data in order to examine the permeability potential along the fault trace, in the area proximal to the fault, and the regional potential (the 8 layers shown in Figure 5). In addition, the MSH study took hot spring geochemistry into consideration, and only used hot springs and fumaroles that were thought to be connected to the magmatic heat source (versus those on the Pumice Plain), and modeled spring proximity weighted by the most recent temperature rather than the maximum temperature (as was done in the statewide model).

The geothermal favorability for the two other play fairway sites, Wind River valley and Mt. Baker, are underway and will incorporate the same data sets and modeling methodology as those outlined for the MSH study area discussed in this paper. Following the completion of the favorability modeling of the other two sites, a data uncertainty and risk analysis will be performed at each site to determine where future efforts will be focused.

## Conclusions and Future Work

The Cascade magmatic arc and the three play-fairway targets within the arc show promise for the first geothermal energy production in Washington State. Innovative 3D permeability modeling techniques, in addition to classic quantitative heat potential modeling, provide insight as to where there is a high likelihood of heat and permeability at 200 m and 3 km depths. After each model's favorability has been assessed, the next step is to perform rigorous uncertainty modeling. This is done to determine where there is high-quality data, and therefore high certainty that the model is representative of the actual conditions, and conversely, it can determine where there is high uncertainty and model outputs need to be amended or more research and data needs to be acquired. The resource potential modeling along with the uncertainty modeling will determine which of the three study areas is the most promising for further exploration. Future efforts will focus on siting temperature-gradient wells and (or) identifying where geophysical data would improve geothermal resource knowledge.

## References

Barker, S. E. and S.D. Malone, 1991. "Magmatic system geometry at Mount St. Helens modeled from the stress field associated with posteruptive earthquakes" Journal of Geophysical Research, v. 96, no. B7, p. 11,883-11,894.

Berri, D. A. and M.A. Korosec, 1983. "Geological and geothermal investigation of the lower Wind River valley, southwestern Washington Cascade Range" Washington Division of Geology and Earth Resources Open File Report 83-5, 48 p., 2 plates.

Blackwell, D. D., 2010. "Updated and combined Regional Heat Flow and Western Geothermal Area databases" Washington State: Southern Methodist University, 1 Excel spreadsheet, accessed Sept. 25, 2010 at http://smu.edu/geothermal/georesou/washingt.htm.

Boschmann, D. E., J.L. Czajkowski, and J.D. Bowman, 2014. "Geothermal favorability model of Washington State" Washington Division of Geology and Earth Resources Open File Report 2014-02, 1 plate, scale 1:900,000, 20 p. http://www.dnr.wa.gov/publications/ger_ofr2014-02_geothermal_favorability.pdf.

Bowman, J. D. and J.L. Czajkowski, 2013. "Washington State seismogenic features database [GIS data]" Washington Division of Geology and Earth Resources Digital Data Series DS-1, version 3.0, http://www.dnr.wa.gov/publications/ger_portal_seismogenic_features.zip.

Burkey, J., 2008. "LOWESS- Locally Weighted Scatterplot Smoothing that does not require the statistical toolbox in matlab" MATLAB release, MATLAB 7.7 (R2008b).

Caine, J.S., J.P. Evans, and C.B. Forster, 1996. "Fault zone architecture and permeability structure" Geology, v. 18, issue 11, p. 1025-1028.

Childs, C., J. Watterson, and J.J. Walsh, 1995. "Fault Overlap Zones within Developing Normal Fault Systems" Journal of the Geological Society, London, v.152, p. 535-549.

Chou, P.C. and N.J. Pagano, 1967. "Elasticity; Tensor, Dyadic, and Engineering Approaches" D. Van Nostrand Company, Inc. Princeton, NJ.

Czajkowski, J. L. and J.D. Bowman, 2014. "Volcanic vents database for Washington State [GIS data]" Washington Division of Geology and Earth Resources Digital Data Series DS-3, version 1.0, http://www.dnr. wa.gov/publications/ger_portal_volcanic_vents.zip.

Czajkowski, J. L., J.D. Bowman, L.A. Fusso, and D.E. Boschmann, 2014a. "Geologic mapping and geothermal assessment of the Wind River valley, Skamania County, Washington" Washington Division of Geology and Earth Resources Open File Report 2014-01, 30 p., 1 plate, scale 1:24,000.

Czajkowski, J. L., J.D. Bowman, L.A. Fusso, and D.E. Boschmann, 2014b. "Thermal and mineral springs database for Washington State [GIS data]" Washington Division of Geology and Earth Resources Digital Data Series DS-7, version 1.0, http://www.dnr.wa.gov/publications/ger_portal_thermal_mineral_springs.zip.

Czajkowski, J. L., J.D. Bowman, L.A. Fusso, and D.E. Boschmann, 2014c. "Washington State geothermal well database [GIS data]" Washington Division of Geology and Earth Resources Digital Data Series DS-8, version 2.0, http://www.dnr.wa.gov/publications/ger_portal_geothermal_wells.zip.

Evarts, R. C., R.P. Ashley, J.G. Smith, 1987. "Geology of the Mount St. Helens area—Record of discontinuous volcanic and plutonic activity in the Cascade arc of southern Washington" Journal of Geophysical Research, v. 92, no. B10, p. 10,155-10,169.

Faulkner, D. R., T.M. Mitchell, E. Jensen, and J. Cembrano, 2011. "Scaling of fault damage zones with displacement and the implications for fault growth processes" Journal of Geophysical Research, v. 116, no. B05403, 11 p.

Ferrill, D.A., J. Winterle, G. Wittmeyer, D. Sims, S. Colton, and A. Armstrong, 1999. "Stressed rock strains groundwater at Yucca Mountain, Nevada", GSA Today, p. 1-7.

Gass, T.E., 1982. "Geothermal heat pumps" Geothermal Resources Council Bulletin, v. 11, no. 11, p. 3-8.

Goepel, K.D., 2013. "Implementing the Analytic Hierarchy Process as a standard method for multi-criteria decision making in corporate enterprises—A New AHP Excel Template with Multiple Inputs" Proceedings of the International Symposium on the Analytic Hierarchy Process 2013.

Hackl, M., R. Malservisi, and S. Wdowinski, 2009. "Strain rate patterns from dense GPS networks" Natural Hazards and Earth Systems Sciences, v. 9, p. 1177-1187.

Huang, S.; and H.N. Pollack, 1998. "Global borehole temperature database for climate reconstruction" National Oceanic and Atmospheric Administration/National Climatic Data Center Paleoclimatology Program Data Contribution Series #1998-044, v. 2001. http://www.ncdc.noaa.gov/paleo/borehole/intro.html.

Jessop, A.M., V.S. Allen, W. Bentkowski, M. Burgess, M. Drury, A.S. Judge, T. Lewis, J. Majorowicz, J.C. Mareschal, and A.E. Taylor, 2005. "The Canadian geothermal data compilation" Geological Survey of Canada Open File 4887, doi:10.4095/220364, http://ftp2.cits.rncan.gc.ca/pub/geott/ess_pubs/220/220364/of_4887.zip.

Karingithi, C.W., 2009. "Chemical geothermometers for geothermal exploration" Short course IV on Exploration for Geothermal Resources, Kenya, Nov., 2009, accessed on 3/6/2015 at: http://www.os.is/gogn/unu-gtp-sc/UNU-GTP-SC-10-0603.pdf.

Keith, T.E. C., T.J. Casadevall, and D.A. Johnston, 1981. "Fumarole encrustations—occurrence, mineralogy, and chemistry" *IN* Lipman, P.W. and D.R. Mullineaux, editors, "The 1980 eruptions of Mount St. Helens, Washington" U.S. Geological Survey Professional Paper 1250, p. 239-250.

Korosec, M.A., 1983. "Geothermal resource targets—progress and proposals" *IN* Korosec, M.A., W.M. Phillips, J.E. Schuster, and others, "The 1980-1982 geothermal resource assessment program in Washington" National Technical Information Service DOE/ET/27014-T6, p. 268-293.

Korosec, M.A., 1984. "Summary of geothermal exploration activity in the State of Washington from 1978 to 1983—Final program report to the U.S. Department of Energy" Washington Division of Geology and Earth Resources Open File Report 84-2, 42 p.

Maerten, L., P. Gillespie, and D.D. Pollard, 2002. "Effects of Local Stress Perturbation on Secondary Fault Development" Journal of Structural Geology, v. 24, p. 145-153.

McCaffrey, R., M.D. Long, C. Goldfinger, P.C. Zwick, J.L. Nabelek, C.K. Johnson, and C. Smith, 2000. "Rotation and plate locking at the southern Cascadia subduction zone" Geophysical Research Letters, v. 27, no. 19, p. 3117-3120.

McCaffrey, R., A.I. Qamar, R.W. King, R. Wells, G. Khazaradze, C.A. Williams, C.W. Stevens, J.J. Vollick, and P.C. Zwick, 2007. "Fault locking, block rotation and crustal deformation in the Pacific Northwest" Geophysical Journal International, v. 169, no. 3, p. 1315-1340.

Muffler, L.J.P., 1993. "Tectonic and hydrologic control of the nature and distribution of geothermal resources" Geo-Heat Center Quarterly Bulletin, v. 15 no. 2, p. 1-10,

Powell, T. and W. Cumming, 2012. "Spreadsheets for geothermal water and gas geochemistry; 3rd ed." Proceedings, Thirty-fifth Workshop on Geothermal Reservoir Engineering, SGP-TR-188, 10 p., http://repository.stategeothermaldata.org/metadata/record/9e15e1a59b768b330 d029e86dc023a37/file/geochemistryspreadsheets-powell-cumming-stanford-2010.pdf.

Saaty, T.L., 2008. "Decision making with the analytical hierarchy process" International Journal of Service Sciences, v. 1, no. 1, p. 83-98.

Sherrod, D.R., W.E. Scott, and P.H. Stauffer, editors, 2008. "A Volcano rekindled—the renewed eruption of Mount St. Helens, 2004–2006" U.S. Geological Survey Professional Paper 1750, 856 p. and DVD-ROM, http://pubs.usgs.gov/pp/1750/.

Shevenell, L., and F. Goff, 1995. "Evolution of hydrothermal waters at Mount St. Helens, Washington, USA" Journal of Volcanology and Geothermal Research, v. 69, p. 73-94.

Smith, R.L. and H.R. Shaw, 1973. "Volcanic rocks as geologic guides to geothermal exploration and evaluation [abstract]" Eos (American Geophysical Union Transactions), v. 54, no. 11, p. 1213.

Thomas, A.L., 1993. "*Poly3D*—a three-dimensional, polygonal-element, displacement discontinuity boundary element computer program with applications to fractures, faults, and cavities in the Earth's crust" M.S. thesis, Stanford University, California.

Washington Division of Geology and Earth Resources, 2010a. "Surface geology, 1:100,000-scale GIS data, June 2010" Washington Division of Geology and Earth Resources, 60.1 M B, http://www.dnr.wa.gov/ ResearchScience/Topics/GeosciencesData/Pages/gis_data.aspx.

Washington Division of Geology and Earth Resources, 2010b. "Surface geology, 1:500,000-scale GIS data, June 2010" Washington Division of Geology and Earth Resources, 12.2MB, http://www.dnr.wa.gov/ ResearchScience/Topics/GeosciencesData/Pages/gis_data.aspx.

Weaver, C.S. and S.W. Smith, 1983. "Regional tectonic and earthquake hazard implications of a crustal fault zone in southwestern Washington" Journal of Geophysical Research, v. 88, no. B12, p. 10,371-10,383.

Weaver, C.S., W.C. Grant, and J.E. Shemeta, 1987. "Local crustal extension of Mount St. Helens, Washington" Journal of Geophysical Research, v. 92, no. B10, p. 10,170-10,178.

Wells, R. E., C.S. Weaver, and R.J. Blakely, 1998. "Fore-arc migration in Cascadia and its neotectonic significance" Geology, v. 26, no. 8, p. 759-762.

Wessel, P., and D. Bercovici, 1998. "Interpolation with splines in tension: a Green's function approach" Mathematical Geology, vol. 30, no. 1, p. 77-93.

Willemse, E.J., D.D. Pollard, and A. Aydin, 1996. "Three-Dimensional analysis of Slip Distributions on Normal Fault Arrays with Consequences for Fault Scaling" Journal of Structural Geology, v. 18 no.2/3, p. 295-309.

Zoback, M.D., 2007. "Reservoir Geomechanics". Cambridge University Press, Cambridge U.K., p. 130-139.